JOURNAL OF MATERIALS SCIENCE **40** (2005) 5733–5739

Pore size analysis of fallow deer (*Dama dama*) antler bone

LOUISE A. EVANS*†, ALAN L. MCCUTCHEON, GARY R. DENNIS, ROBERT C. MULLEY, MICHAEL A. WILSON
College of Science, Technology and Environment,University of Western Sydney, Locked Bag 1797, Penrith South DC, NSW 1797, Australia
E-mail: Louise.Evans@uts.edu.au

Published online: 25 August 2005

Deer antler is of interest to material scientists because it represents bone which can withstand applied stresses of over 300 MPa. In this work we demonstrate the presence of nanopores in this material by nuclear magnetic resonance (NMR) spectroscopy, and gas adsorption and mercury intrusion experiments. It is also shown that organic material in the antler influences observed pore sizes. Different modal groups of pores were observed when organic lipid material was removed from the sample and the sample saturated with water. The dominant organic phase associated with the small pores is protein.

1. Introduction

Biomineralized tissues are a complex arrangement of organic and inorganic components. In bone, for example, up to seven hierarchical levels of structure have been identified [1] with typical dimensions ranging in scale from 1.5 nanometres for the diameter of the triple helical tropocollagen filament through to millimetre or larger dimensions for the bone macrostructure [2]. Within these tissues, pore size and interconnectivity of the pores are vitally important factors since they affect strength and other mechanical properties of the material in addition to allowing nutrient diffusion and cell attachment during growth and in natural repair processes [3].

Antler either in the form of velvet or as fully calcified tissue has been used in Chinese medicine for at least 2000 years; its use in western medicine is gaining in popularity as people strive to minimise the ingestion of chemicals and genetically modified foodstuffs [4–6]. Like all bone samples, the primary inorganic component of mature deer antlers is a carbonated apatite interwoven with a collagenous organic matrix. However, deer antler is a unique example of long bone formation in as much as it shows extremely rapid formation of preosseous tissue (up to 2 cm per day) including nerve cells and vascular channels [6]. Indeed, these tissues are the only mammalian bone structure that is shed and regenerates completely every year [7]. The complex array of cavities within mineralized structures is usually oriented to optimize fracture mechanics of the material [8].

Traditionally, the microarchitecture of biomineralized structures has been examined directly using transmission electron microscopy or indirectly using "molecular probes" such as the electron-dense iron-storage protein ferritin, whose diameter of 12–13 nm allows penetration of the many channels and cavities within these tissues [9], or gas adsorption and mercury intrusion experiments or proton NMR relaxation measurements [10–12]. These measurements are particularly useful for probing fine structure including pore dimensions at the nanometer level. Here we study fallen hard antler samples from a three to four year old pasture-fed fallow deer buck (*Dama dama*). Deer antler must be extremely tough; before casting, fully calcified antler can withstand applied stresses of over 300 MPa, at least 100 MPa higher than that of mammalian femur [2]. Spin-spin relaxation times (T_2's) have been measured on the antler remains and as a function of wetting and dewatering. The distribution of T_2's has been interpreted in the first instance as pore size distributions. The effects of removing both lipid and proteinaceous material on pore size distributions have also been studied.

2. Materials and methods

2.1. Sample collection

Fallen hard antler samples from a three to four year old pasture-fed fallow deer buck (*Dama dama*) were collected after antler casting which occurs in the period September/October in the southern hemisphere. The

*Author to whom all correspondence should be addressed.
†*Present Address*: Department of Chemistry, Materials and Forensic Science,University of Technology, PO Box 123, Broadway 2007, Sydney, NSW Australia.
0022-2461
DOI: 10.1007/s10853-005-1118-5

fully calcified samples were allowed to dry extensively at ambient temperature before being sectioned transversely. Note that for this series of experiments both the antler tip and trez tine were removed and only main beam tissue was used. Subsequently, the upper portion of the antler was used for analysis (length of sample approximately 8 cm). Hence water could access the internal structure from both ends of the sample and from the porous surface formed by removal of the trez tine.

2.2. Sample treatment

Although the sample appeared to be dry when received, approximately 2 g of water were able to be removed following overnight treatment in a vacuum dessicator (final mass of sample 32.9275+/0.05 g). Once the dry mass of tissue had been accurately determined, the sample was water saturated by immersing the sample in approximately 500 mL of water, applying a vacuum (rotary pump) for 5 min and then purging with nitrogen for a further 5 min This process was repeated a further three times. The sample was then removed quickly, the external surfaces dried and the sample again weighed accurately to the significant figures noted above. The entire procedure was repeated until the mass of the water saturated antler was constant. The saturated sample was then wrapped in teflon tape to prevent water loss during the measurements, and immediately placed in the NMR chamber for analysis.

In order to determine the effects of lipid and proteinaceous material on the pore size and interconnectivity, these components were sequentially removed by chemical extraction and the NMR water saturation analysis repeated after each extraction process. For lipid removal, the sample was treated with diethyl ether in a soxhlet extractor for approximately 12 hours. Protein was removed according to the method of Frayssinet *et al.* [14], which uses hydrogen peroxide extraction followed by treatment with 1 M NaOH solution.

2.3. Infra red spectroscopy

In order to confirm efficacy of the organic extraction techniques, infrared spectra were recorded on the as received sample and after each chemical treatment step. Approximately 2 mg of sample corresponding to the trabecular (spongy) region was carefully removed using a microscope and scalpel. This was then ground with KBr and pressed into 13 mm pellets. FT-IR spectra were recorded on a Biorad FTS 3000 MX instrument.

2.4. Nuclear magnetic resonance spectroscopy

Proton nuclei relaxation processes were recorded on a Resonance Maran 2 broadline NMR spectrometer. This instrument utilizes a large permanent magnet producing a low intensity field with a Larmor frequency of 2.1 MHz. Relaxation measurements were recorded using the Carr-Purcell-Meiboom-Gill (CPMG) pulse sequence [15, 16] with a series of pulses separated by a delay time, τ, of 150 μs. The pulse length was set to 27.5 μs and a sequence repetition time of 2 s was used. The number of scans collected was usually 256. After an initial $\pi/2$ pulse, a series of π pulses at τ, 3τ, 5τ, nτ μs etc. were applied to produce a series of echoes at 2τ, 4τ and 6τ etc. which decrease exponentially with time constant, T_2. Using this technique the effect of diffusion is kept minimal by keeping short the interval between the pulses so that T_2 for each pore can be derived from the multiple simple Bloch equation [15–17] as:

$$M_t = \sum_i A_i \exp(-t/T_{2i}) \quad (1)$$

where M_t is the observed signal, A_i is a constant reflecting the contribution of each type of pore to the relaxation behaviour, t is time and T_{2i} are the various T_2 values needed to fit the decay in signal. In principle if T_{2i} values are known, pore size distributions can be measured by fitting values for M_t to obtain A_i. In practice, they are best fitted through integration over a continuous T_2 from values equal to zero to those for the bulk solution. In this data there is the presence of noise, ε.

Thus

$$M(t) = \int_{T_2=0}^{T_2 bulk} A(T_2 \exp(-t/T_2))d(T_2) + \varepsilon(t) \quad (2)$$

The magnitude of A is interpreted as the number of pores if the pore geometry is known. T_2 is interpreted as pore size. To extract A values from this equation weighting constants are applied with least squares minimisation techniques applicable to NMR measurements of this kind [16]. The weighting constants used in this study were in the range of 0.01 to 0.15 since they gave best fit.

To calculate the pore size from a knowledge of the melting point depression of water, a modified Kelvin equation (also known as the Gibbs-Thompson equation) was used [18, 19]:

$$\Delta T = T_m - T_m^x = \frac{4\sigma T_m}{\Delta H_f \rho_s x} \quad (3)$$

where T_m is the melting point of bulk water (273.15 K), T_s^x is the melting point of water in pores of diameter, x, σ is the surface tension of water (75.64 mN m^{-1} = 7.564 $\times$ 10^{-2} J m^{-2}), ΔH_f is the bulk enthalpy of fusion of water (333.6 J g^{-1}), ρ_s is the density of ice (at the temperature measured) and x is the pore diameter. If ρ_s has units of g cm^{-3}, then a value of x will be obtained with units of μm. It may be seen from Equation 3 that as long as the temperature is held constant below normal (bulk) melting point, then ΔT will be inversely proportional to pore diameter. A proportionality constant relating the relaxation time, T_2, to pore diameter can then be determined from the NMR spectrum obtained at the depressed temperature by noting the T_2 value separating frozen from nonfrozen water.

In the current study, the delipidated and deproteinated sample was saturated with water and then frozen at a number of known temperatures. To ensure constant temperature was being maintained throughout the NMR measurements, temperature was monitored with a platinum resistance thermometer. After recording these NMR spectra with most of the water in a frozen state, the T_2 value which separates the frozen and liquid water was noted for calibration purposes. Errors associated with this methodology have been discussed elsewhere [20].

To follow water loss from the antler by evaporative processes, NMR analyses were repeated every 45 min and a series of measurements acquired over approximately 30 h. For this investigation 1024 scans were used for each measurement. Scans for initial measurements were obtained with the samples wrapped in teflon since this polymer does not give an NMR signal.

2.5. Gas adsorption and mercury porosimetry

Sample size was a limiting factor for preparation of samples of these materials for gas adsorption and mercury intrusion because the dimensions of the sample tube is 9 mm radius and a length of 2 cm, but the dimensions of a cross section of the antler greatly exceeded these limits. Two representative samples of the cortical bone were cut from the untreated and deproteinated antler, and any trabecular tissue was removed with a scalpel. Sampling of the trabecular material was not attempted because it was expected that cutting of this softer, spongy material would affect the inherent pore structures.

Gas adsorption and desorption isotherms using nitrogen (73.35 K) were measured using a Micrometrics Tristar 3000. The desorption data was analysed using the Barrett, Joyner and Halenda (BJH) method to obtain the pore size distributions. Mercury intrusion experiments (Micrometrics Autopore IV 9500) were completed on the same samples to gain a second estimate of pore size distribution.

3. Results

3.1. Infrared spectroscopy

The infrared spectrum of the untreated sample showed bands due to carbonate and phosphate groups from the inorganic apatitic phase, and from carboxylate groups of the organic matrix (Fig. 1a). Most notably, carbonate ν_2 and ν_3 vibrational modes were apparent at about 875 cm^{-1} and at 1500–1400 cm^{-1} respectively while phosphate bands appeared at about 960, 1100–1000 and 600–550 cm^{-1} (phosphate ν_1, ν_3 and ν_4 respectively). All of these bands arise from groups in the apatite crystal lattice. A weak band at about 2932 cm^{-1} due to a C-H stretching mode combined with the presence of an absorption band at 1647 cm^{-1} corresponding to amide C=O groups confirmed the presence of organic components in the sample. The broad absorption band from 3600 to 3000 cm^{-1} corresponds to adsorbed water.

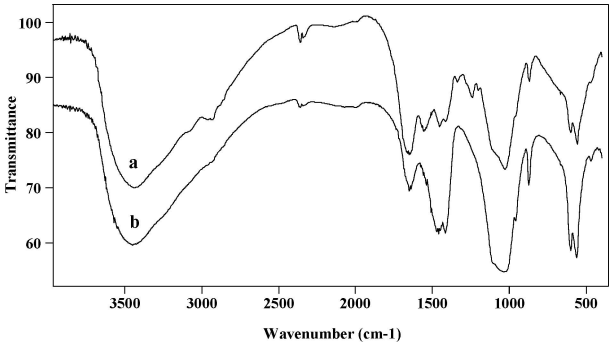

Figure 1 Fourier transform infrared spectra of (a) untreated and (b) delipidated and deproteinated antler bone.

It should be noted that the spectrum resembles closely that of a typical mammalian bone sample [21].

Following removal of the lipid fraction by ether extraction the infrared spectrum did not alter significantly from that of the untreated sample (data not shown), however 0.06 g of an oily substance, presumably lipid, was recovered upon evaporation of the ether extract. Note that values of 2 to 5% fat have been reported for freshly fallen antlers of other deer species [22]. The spectrum obtained following protein oxidation by hydrogen peroxide showed that the C-H band at 2932 cm^{-1} had disappeared and that there had also been a large reduction in relative magnitude for the amide I band at 1647 cm^{-1} and loss of the amide III band at 1240 cm^{-1} (Fig. 1b), confirming that the process was effective in removing a major portion of the protein constituent. Thus it can be concluded that significant amounts of protein remain in the structure following antler casting and natural dehydration processes. Following delipidation and deproteination the sample was a consistent off-white colour throughout both cancellous and cortical components with no evidence of reddish brown colouration characteristic of organic residues.

3.2. Pore size calibration

Fig. 2 shows a sample NMR spectrum for one of the depressed temperatures (251.35 K) which corresponds to a pore diameter of 10.9 nm. The average proportionality constant relating T_2 to pore diameter was thus found to be 177 ± 20 $\mu s\ nm^{-1}$.

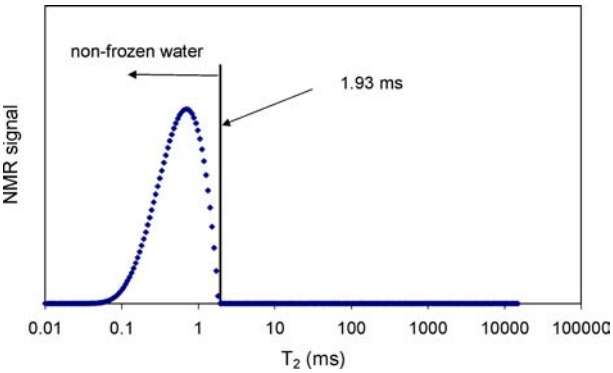

Figure 2 Modal distribution peak for nonfrozen water in the pores at 251.35 K.

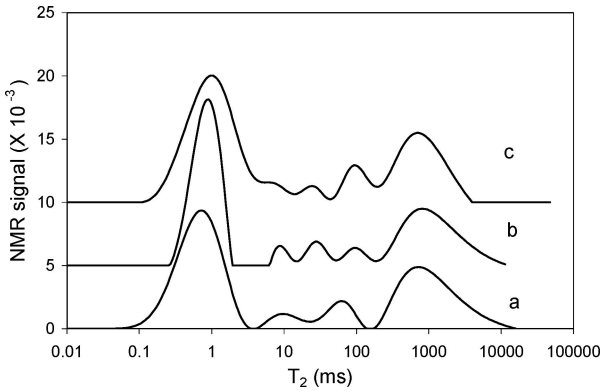

Figure 3 Representative distribution of T_2 relaxation times for pores in (a) untreated (b) delipidated and (c) delipidated and deproteinated antler bone.

3.3. Pore size distribution

NMR spectroscopy of the untreated antler, without water saturation, showed a single modal peak with a T_2 value of about 730 μs presumably due to water trapped in very small pores (data not shown). Once the sample had been treated by vacuum dessication, no NMR signal was apparent, confirming that this peak is due to trapped water and not from any residual organic material. Indeed, typical values of 50 μs for bone collagen have been reported [23]. Following water saturation three additional peaks were observed at 9.9, 64.5 and 770 ms (0.06, 0.36 and 4.35 μm) (Fig. 3a). In addition, enhancement of the peak at 730 μs (4.1 nm) was also apparent.

Following delipidation and deproteination it was noted that T_2 distributions in the intermediate range of about 10 to 100 ms changed, presumably as some pores are destroyed by the treatment and new pores are revealed (Figs 3b and c). These occurred at T_2 values of 28.6 and 101 ms corresponding to diameters of 0.15 and 0.54 μm respectively (Fig. 4). Percentage distribution of the pores has been calculated by determining the area under each peak; the values for the smallest and largest pores are shown on Fig. 4. Pores in the intermediate range accounted for approximately 10% of the total pores in the sample. The modal peak with an initial T_2 value of 730 μs for the untreated sample moved to increasing longer T_2 values with sequential removal of organic material. Pores producing a modal peak with a T_2 value of 770 ms showed little affect after treatment. The pore diameter corresponding to this peak ($\sim$4 μm) correlates well with literature values for osteocytic lacunae (see below).

The mercury intrusion and nitrogen adsorption data for the cortical bone (Fig. 5) showed that nanosized pores are present in the untreated cortical bone (pore sizes of 2.0, 2.5 and 3.2 nm (N_2), and 3.3 and 4.0 Hg). These results agree well with the pore size calculated for the large peak with a T_2 value of 730 μs, i.e. 4.1 nm. The data for the treated cortical bone (broad distributions at 10 nm (N_2), and 3 nm (Hg)) confirmed that there is significant changes to the pore structure of the antler after removal of lipids and proteins.

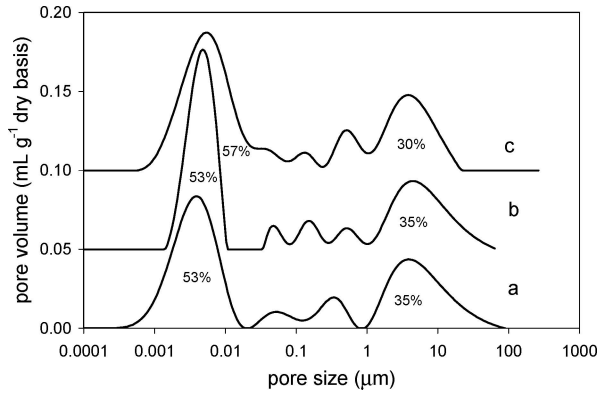

Figure 4 Relative distribution of water as a function of pore diameter calculated using the modified Kelvin equation. Measurements are shown for (a) untreated (b) delipidated and (c) delipidated and deproteinated antler bone.

3.4. Rates of water evaporation

Rates of water loss from the treated and untreated sample are shown in Figs 6–8. For the purposes of this report three types of pore have been defined: small (0.5 to 20 nm), intermediate (20 to 890 nm) and large (890 nm to 90 μm). Note that these values differ from the IUPAC definitions of micro-, meso- and macropores. Data has been shown for those pores containing the largest proportions of water (small and large size); data has not been provided for the minor intermediate pore size range because of the associated significant relative error. Most notably, for this series of experiments rate of water loss was different from the large pores in the delipidated and deproteinated sample (Fig. 8). There did not appear to be any appreciable difference between any of the rates for the smaller pores (Fig. 7). It was also noted that there had been complete water loss from the large pores by about 22 hours, whereas water was still present in the smaller pores at this time (compare Figs 7 and 8).

4. Discussion

4.1. Comparison between pore size methods

Several authors have used magnetic resonance cryoporometry techniques with success particularly in the mesopore range of 3 to 100 nm [26–28]. Our results show it is important to calibrate this methodology with other techniques because of the inherent NMR assumptions discussed concerning symmetry of the pores [20]. For example, when Wang and Ni [26] assessed cortical porosity and pore size distribution in human bone as a means for detecting age related changes to bone, they used a histomorphometry technique rather than cyroporometry for calibration of pore size as a function of T_2. Although they measured three peaks in the T_2 distribution for their sample ($T_2 \sim$ 1.6, 52 and 800 ms), they only found two peaks using optical image analysis (pore sizes 3.9 and 58 μm). They assumed that the smaller pore size, 3.9 μm, must be related to the 1.6 ms peak, and the 58 μm pore corresponds to the 52 ms signal. No assignment was given for the 800 ms value of T_2. The cryoporometry, nitrogen adsorption

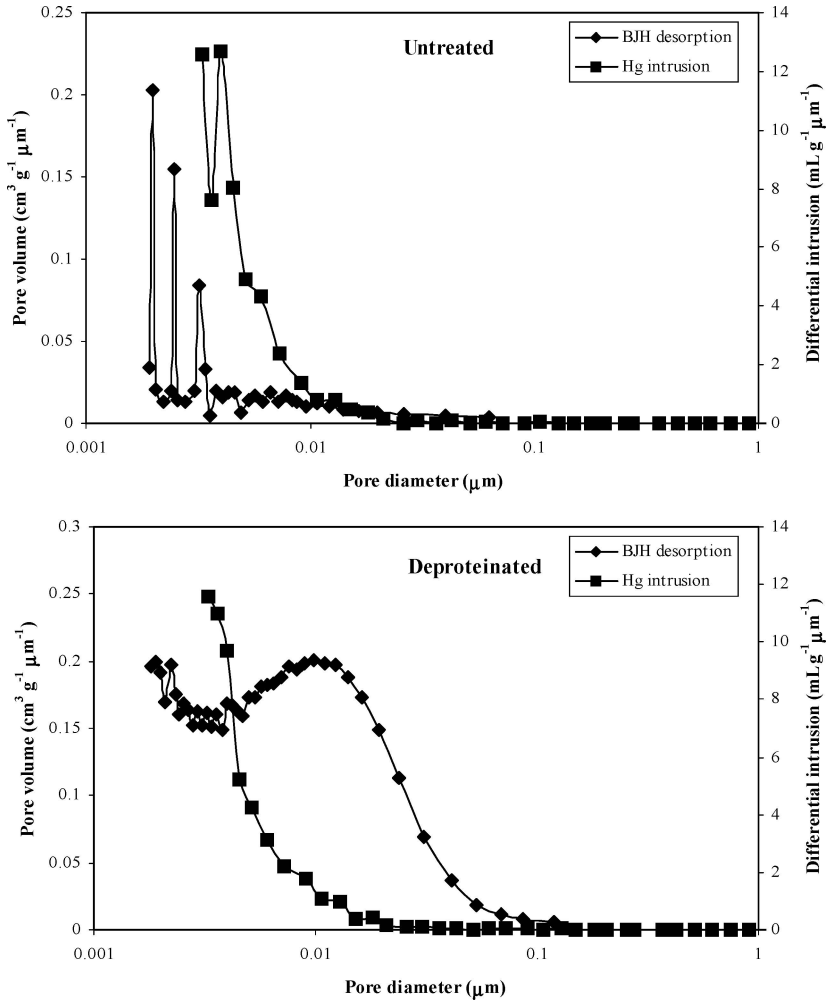

Figure 5 Pore size distributions from nitrogen adsorption (BJH) and mercury intrusion (Hg) experiments.

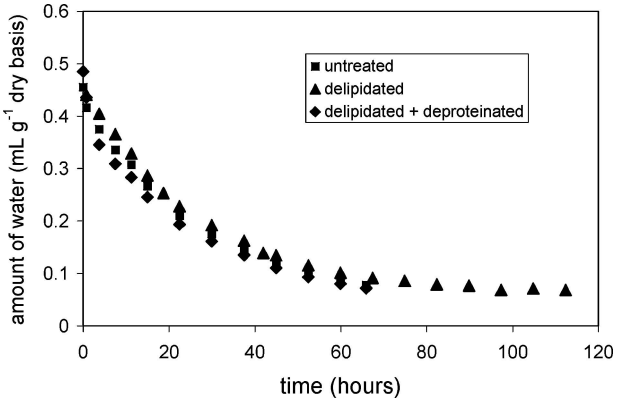

Figure 6 Graph of total evaporative water loss with time.

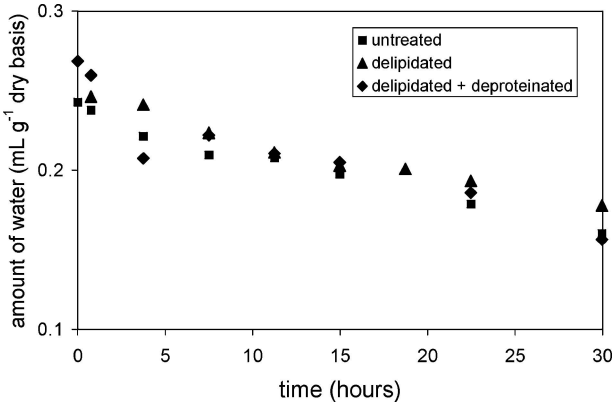

Figure 7 Graph of evaporative water loss with time from small (0.5 to 20 nm) pores.

and mercury intrusion results, however, show that this was an incorrect deduction and that the 1.6 ms peak would be due to nanosized pores.

In summary different pore size measurements measure different things and it is inappropriate to correlate them eg with goodness of the fit tests.

4.2. Origin of pores

Fallen antler contains several structural layers [5] which at the gross level are analagous to the cortical and trabecular strucures found in other mammalian bone structures. Trabecular (spongy) bone has a very open structure with some voids ranging from 200 to 400 μm, a value similar to that observed in the SEM for the antler sample analysed here (data not shown) but outside the range of the NMR technique presented here since water in such large pores behaves in the same way as bulk water. In cortical (compact) bone the largest channels are the Haversian and Volkmann's canals ($\sim$50 μm) which contain blood vessels and nerves. Thus these structures may be responsible for the asymmetry of the last modal peak (highest T_2 distributions). At the other

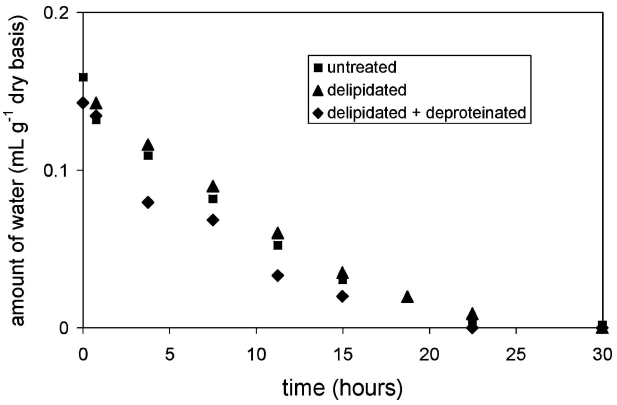

Figure 8 Graph of evaporative water loss with time from large (0.89 to 90 μm) pores.

end of the scale, the smallest cavities which have been proposed in undeproteinated bone are gaps of approximately 35 nm between the N-terminus of one triple helical collagen molecule and the C-terminus of the next [1]. However, removal of the organic matrix would necessarily create larger cavities in the microstructure (of the order of 85 nm). The results in Fig. 4 suggest some change in the nanometer range of pores although there is no evidence of a change to around 85 nm. Rather it appears removal of lipid sharpens the distribution but deproteination broadens it again. In the antler sample examined here approximately 50% of the pores were identified in the range of 1 to 10 nm; extremely small dimensions which are probably associated with porosity arising from spaces around organic matrix fibres.

Much larger holes within the bone microstructure are lacunae and canaliculae that contain bone cells (osteocytes) and their protrusions. Average diameters of 5 μm have been reported for osteocyte lacunae [12] with the interconnecting canaliculae tunnels being an order of magnitude smaller. Thus lacuno-canalicular dimensions are well within the range discernible using the current methodology. A change of pores from 0.06 and 0.36 μm to 0.15 and 0.54 μm is consistent with remnant cellular residue being removed by solvents.

4.3. Pore contaminants

The dominant organic phase associated with the small pores would appear to be protein, since lipid removal caused no change in peak area but subsequent deproteination caused an increase in relative distribution of these pores and hence a decrease in the apparent number of large pores. The observation that removal of the lipid caused a redistribution of T_2's in the intermediate size range (canalicular level porosity) could be due either to unblocking of some pores to become physically larger or to removal of hydrophobic material to expose hydrophilic polar sites making the activation energy for water loss higher and affecting T_2. However, an increase in energy is not consistent with the evaporation results for the small pores. These pores have a larger relative surface area than the intermediate pores and hence an increase in energy at the surfaces of small pores should lead to a greater retardation of evaporation. Since removal of organics from small pores had negligible effect on rates of evaporation it must be concluded that the dominant factor in these pores is one of neck shape rather than surface changes. Also noteworthy in the water evaporation experiments is that although the large pores became essentially dry at about 22 h, the small pores continued to lose water until they approached the same amount of water found in the as received sample (6.2% v/w). Thus the rate of water loss at this point had reached an equilibrium value beyond which further water removal from the small pores is not energetically favoured.

5. Conclusions

1. Good correlations have been found between pore size measurements on fallen hard antler samples from a three to four year old pasture-fed fallow deer buck (*Dama dama)* by nuclear magnetic resonance (NMR) spectroscopy, and gas adsorption and mercury intrusion experiments.

2. Nanosized pores (0.001 to 0.01 μm) have been observed in samples of the above origin.

3. Lipid and protein removal suggests some change in the nanometer range of pores. Rather it appears removal of lipid sharpens the distribution but deproteination broadens it again. In the antler sample examined here approximately 50% of the pores were identified in the range of 1 to 10 nm; extremely small dimensions which are probably associated with porosity arising from spaces around organic matrix fibres.

4. The dominant organic phase associated with the small pores would appear to be protein. Since removal of organics from small pores had negligible effect on rates of evaporation it must be concluded that the dominant factor in evaporation from these pores is one of neck shape rather than surface changes. Also noteworthy in the water evaporation experiments is that although the large pores became essentially dry at about 22 h, the small pores continued to lose water until they approached the same amount of water found in the as received sample (6.2% v/w). Thus the rate of water loss at this point had reached an equilibrium value beyond which further water removal from the small pores is not energetically favoured.

5. Larger pores 0.06 and 0.36 μm are also observed in the antler. These evaporate water rapidly as expected and removal of organic material increases their size also as expected.

References

1. S. WEINER and H. D. WAGNER, *Annul. Rev. Mater. Sci.* **28** (1998) 271.
2. S. MANN, "Biomineralization: Principles and Concepts in Bioinorganic Chemistry" (Oxford University Press, New York, 2001).
3. R. Z. LEGEROS, *Clinical Orthopaedics and Related Research* **395** (2002) 81.
4. R. GOSS, "Deer Antlers: Regeneration, Function and Evolution" (Academic Press, New York, 1983).
5. C.-H. CHO, Y.-A. WOO, H.-J. KIM, Y.-J. CHUNG, S.-Y. CHANG and H. CHUNG, *Micro. J.* **68** (2001) 189.

6. Y. C. KONG and P. P. H. BUT, in: Biology of Deer Production, edited by P.F. Fennessy and K. R. Drew, The Royal Society of New Zealand. *Bulletin* **22** (1985) 311.
7. H. J. ROLF and A. ENDERLE, *Anat. Rec.* **255** (1999) 69.
8. J. D. CURREY, *J. Biomech.* **36** (2003) 1487.
9. L. A. EVANS, D. J. MACEY and J. WEBB, *Acanthopleura hirtosa.* Acta Zoologica (Stockholm) **75** (1994) 75.
10. P. FANTAZZINI, C. GARAVAGLIA and G. GUGLIELMI, *Magn. Reson. Imaging* **19** (2001) 477.
11. S. CAPUANI, F. M. ALESSANDRI, A. BIFONE and B. MARAVIGLIA **14** (2002) 3.
12. P. FANTAZZINI, R. J. S. BROWN and G.C. BORGIA, *Magn. Reson. Imaging* **21** (2003) 227.
13. Q. NI, J. D. KING and X. WANG, *Meas. Sci. Technol.* **15** (2004) 58.
14. P. FRAYSSINET, N. ROUQUET, D. MATHON, A. AUTEFAGE and J. FAGES, *Biomat.* **19** (1998) 2247.
15. H. Y. CARR and E. M. PURCELL, *Phys. Rev.* **94** (1954) 630.
16. S. MEIBOOM and D. GILL, *Rev. Sci. Instrumen.* **29** (1958) 688.
17. K. R. BROWNSTEIN and C. E. TARR, *Phys. Rev. A* **19** (1979) 2446.
18. R. SCHMIDT, E. W. HANSEN, M. STOCKER, A. AKPORIAYE and O. E. ELLESTAD, *J. Am. Chem. Soc.* **117** (1995) 4049.
19. J. H. STRANGE and M. RAHMAN, *Phys. Rev. Letters* **71** (1993) 3589.
20. A. L. MCCUTCHEON, M. A. WILSON, B. HARTUNG-KAGI and O. KHIAM, *J. Phys. Chem.* B **106** (2002) 2928.
21. R. Z. LEGEROS, J. P. LEGEROS, O. R. TRAUTZ and E. KLEIN, *Dev. Appl. Spectrosc.* **7** (1970) 3.
22. N. N. PATHAK, A. K. PATTANAIK, R. C. PATRA and B. M. ARORA, *Small Rumin. Res.* **42** (2001) 61.
23. Y. WU, J. L. ACKERMAN, D. A. CHESLER, L. GRAHAM, Y. WANG and M. J. GLIMCHER, *Magn. Reson. Med.* **5** (2003) 59.
24. S. C. COWIN, *J. Biomech.* **32** (1999) 217.
25. P. FANTAZZINI, V. BORTOLOTTI, R. J. S. BROWN, M. CAMAITI, C. GARAVAGLIA, R. VIOLA and G. GIAVARESI, *J. Appl. Phys.* **95** (2004) 339.
26. X. WANG and Q. NI, *J. Orthop. Res.* **2** (2003) 312.
27. S. M. ALNAIMI, J. H. STRANGE and SMITH, *Magn. Reson. Imaging.* **12** (1994) 257.
28. P. FANTAZZINI, R. VIOLAR, S. M. ALNAIMI and J. H. STRANGE, *ibid.* **19** (2001) 481.

Received 27 November 2004
and accepted 22 March 2005